2023 IEEE International Conference on Robotics and Automation (ICRA 2023)
May 29 - June 2, 2023. London, UK

A Tactile-enabled Hybrid Rigid-Soft Continuum Manipulator for Forceful Enveloping Grasps via Scale Invariant Design

Ian H. Taylor Maheera Bawa Alberto Rodriguez
Massachusetts Institute of Technology

***Abstract*— This work presents a novel hybrid rigid-soft continuum manipulator, which integrates high-resolution tactile sensing in a form factor that is forceful, compliant, inherently safe, and easily controllable. We utilize a hybrid approach motivated by scale-invariant principles to fuse the rigid and soft design domains while addressing their respective challenges. We use Euler-Bernoulli beam theory and geometric inference to design and develop a novel variant of folded flexure hinge (FFH) compliant mechanism, the variable area moment of inertia folded flexure hinge (VAFFH), which deforms logarithmically along its length and thus yields first-order scale-invariant grasp behavior. Finally, we characterize the forcefulness of the manipulator and demonstrate its compliance, adaptability, and tactile sensing capabilities in selected tasks.**

I. Introduction

Rigid and soft approaches to robotic manipulator design each offer unique advantages and challenges. Soft designs often utilize the compliance of their hyper-elastic structures to provide an "embodied intelligence" in the form of passive adaptationg to the contours of complex objects and enable stable and inherently safe behaviors with simple control inputs. However, the root of this intelligence, the complex behaviors that hyper-elastic materials exhibit (non-linearity, hysteresis, visco-elastic effects, large strain or deformation), pose significant design challenges, often resulting in reduced kinematic controllability due to a lack of accurate models and difficulty in sensorization due to a lack of sufficient rigid mechanical structure [1], [2], [3], [4].

Conversely, rigid approaches enable robust actuation and higher-resolution methods of tactile feedback. Yet, compliance and adaptability are less often inherent. Unless specifically addressed during the design process, compliant and adaptable behavior can often only be enabled from within the control domain, usually at the cost of utilizing complex and computationally demanding control schemes. Additionally, purely rigid grasping, while versatile, struggles significantly in scenarios that require the application of large wrench forces, for example in a human environment where many objects have handles that require such force for operation and control. Because contacts between objects and the manipulator's structures are often limited to line or point contacts, grasps slip easily under said forces due to the inability to maintain force closure [5], [6].

This work presents an approach that bridges the gap between the rigid and soft design paradigms by utilizing scale-invariant principles. We demonstrate a continuum manipulator that is simultaneously forceful, inherently safe, compliant, and easily controllable, all while integrating high-resolution tactile feedback. We present three main contributions.

- **Variable Area Moment of Inertia Folded Flexure Hinge (VAFFH):** We develop a novel variant of the serpentine folded flexure hinge compliant mechanism that utilizes an area moment of inertia which varies along the hinge's extrusion axis. The specification of this mechanism defines the work envelope and minimum energy configurations of the continuum manipulator and enables the approximation of scale-invariant compliances within its elastic regions (Section III).
- **Continuum Manipulator:** We describe the design, fabrication, and assembly of a fully-functioning tendon-driven continuum manipulator composed of an elastic exoskeleton and hyperelastic elastomer with embedded vision sensors. Additionally, we demonstrate design methods to mitigate common challenges introduced by hyperelastic materials commonly used in soft robotic applications (Section III).

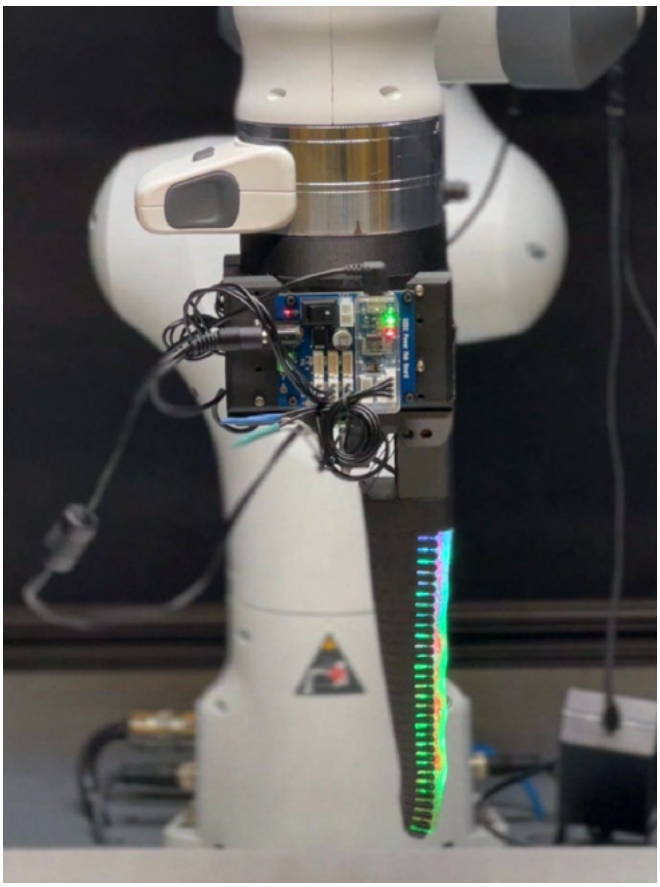

Fig. 1: The continuum manipulator attached to a Franka Emika panda robot. The hybrid rigid-soft construction enables the ability to vary the stiffness of the manipulator in its various configurations. In this case, the manipulator has been stiffened to act as a palm.

979-8-3503-2365-8/23/$31.00 ©2023 IEEE

Fig. 2: Continuum manipulators with a tapered profile and helical grasp geometry found in nature. *From left to right:* elephant trunk [7], chameleon tail [8], octopus tentacle [9], seahorse tail [10], and carnivorous plant tendril [11].

- **Grasp Analysis:** We experimentally evaluate the functionality and forcefulness of the enveloping grasps and unique behaviors enabled by the continuum manipulator. Additionally, we demonstrate the use of integrated high-resolution tactile sensing to enable force and slip feedback across multiple contact patches (Section IV).

II. Related work

Within robotics, continuum manipulators have long been an active field of study [3]. By utilizing a serial arrangement of rigid links, a continuum body, or hybrid structure, combined with a selected method of actuation, typically embedded fluids, tendons, smart materials, or electromagnets; high degrees of freedom are achieved in a structure whose constitutive material can be actuated to form curves with continuous tangent vectors [4], [12]. This unique configuration enables a variety of dynamic behaviors and methods of manipulation.

A common method of manipulation involves wrapping the manipulator around an object in an enveloping grasp [13]. If the structure of the manipulator has a sufficiently low mechanical impedance it will adapt and conform to the object's morphology, grasping it firmly without damage or slippage. This can be seen in "trunk" or "tentacle"-like manipulators. For example, the helical contractile pneumatic artificial muscle manipulator described by Guan et. al. or Festo's pneumatic octopus arm-inspired soft actuator [14], [15]. Another method utilizes the high degrees of freedom of these manipulators to efficiently navigate around obstacles and inspect congested spaces [3]. This behavior is particularly useful in medical applications where they can be used to perform minimally invasive procedures [16]. Continuum manipulators utilized for medical procedures are often constructed to have an open lumen to allow for small surgical tools to be passed through to the accessed area. Kutzer et al. and Du et. al.[17], [18] demonstrate such tendon-actuated manipulators composed of a super-elastic nitinol continuum which have been notched to create a shape-similar (i.e. constant-pitch), solid notch hinge. This type of compliant mechanism, also known as the serpentine flexure hinge or folded flexure hinge (FFH), enables precise and controllable large strain continuum motion. While traditional FEA techniques have been used to model the in-plane elastic response of an FFH with few segments, it is often more practical to design and model longer segments and their resultant minimum energy deformed configuration using purely geometric analysis which is later validated [19], [20].

Sensorization of continuum manipulators poses a particular challenge requiring innovative solutions due to the incompatibility between the compliant body of the manipulator and typically rigid sensing components. Capacitive and resistive methods are often used due to their compact form factors and straightforward implementation which comes at the cost of sensing resolution [21]. Conversely, optical methods enable high-resolution tactile feedback yet require an underlying "skeleton" to provide structure, so that rigid and soft components may be joined together [22].

Continuum manipulators are often described analogously to biological structures (in particular trunks, tentacles, tails, and tendrils as seen in Fig. 2) and biological inspiration is usually cited as the progenitor of their dynamic capabilities [15], [21], [14], [13], [3], [4]. Digging further into this biological inspiration, we see that many biological systems across disparate ecological domains have evolved towards tapered limbs that utilize helical and spiral-like grasp behaviors as methods of manipulation. The tapered structure of these limbs describes a function that scales limb diameter linearly along the length of the limb, resulting in a logarithmic change in stiffness (assuming an approximately isotropic body). This compliance gradient efficiently enhances the distal flexibility of the limb without sacrificing the power of the proximal regions [15]. The result is a limb that is efficiently adaptable to a wide variety of objects and maintains the appropriate amount of power, and flexibility necessary regardless of the object's size. In effect, the manipulator's grasp behavior is "scale invariant". Rodriguez et al.[23] formulate this principle analytically and develop a generalized model of invariant grasps to subsequently guide continuum manipulator design. This principle of grasp invariance not only greatly enhances the adaptability of the manipulator but also, under specific conditions, gives rise to the logarithmic spiral-shaped manipulators so often seen in nature.

III. Design and Fabrication

We design a tactile sensing-enabled continuum manipulator that is simultaneously forceful and compliant while integrating a stiffness profile that enables approximately logarithmic deformation and thus highly adaptable and scale invariant grasp behaviors. Additionally, we formulate the design such that its behavior is easily and predictably controlled via simple control schemes.

A. Design of the VAFFH

We select amongst current approaches of continuum manipulator structure and opt to use a hybrid tendon-actuated exoskeleton-covered soft continuum layup as the basis of our design. As She et al.[22] demonstrated, this is one of the few configurations that can compatibly integrate optical-based high-resolution tactile sensing. Additionally, the exoskeleton enforces a constrained work envelope on the hyper-elastic continuum sensing region, reducing kinematic uncertainty during operation. Through proof of concept prototypes, we find that the exoskeleton's geometry is the primary determinant of the manipulator's minimum energy configurations. Due to the low mechanical impedance of the soft internal continuum, it is unable to resist any deformation induced by the exoskeleton, and thus does not substantially modulate the exoskeleton's stiffness profile. We opt to utilize a serpentine FFH design to enable compliance within the exoskeleton due to its compact form factor, ability to transmit large forces and maintain large deformations under elastic loading conditions [20], [17], [18]. These compliant hinges, in contrast to discrete revolute hinges, provide the ability to tune and optimize their compliance behaviors via their geometric parameters [19].

To enforce approximately logarithmic deformation in the manipulator, the flexure hinge must deform helically under in-plane elastic loading. Assuming isotropic material and constant area moment of inertia, a shape-similar FFH will deform approximately equivalent to an analogous series of revolute hinges, where each notch of the FFH acts as a discrete joint actuated by a linear spring. Thus the minimum energy deformed configuration can be approximated geometrically by utilizing a forward kinematic approach while maintaining a non-penetration constraint [19], [18]. For the proposed case, the fully deformed configuration of an FFH with n number of segments will approximate a polygon with the same number of sides and the compliance will be equivalent to a series summation of the spring stiffnesses. Thus as $n \Rightarrow \infty$ the FFH more closely approximates a circle while the stiffness profile remains constant along its length.

A spiral can be described in polar coordinates as $r = r(\phi)$ where the radius r is a monotonic continuous function of angle ϕ. As such, a circle represents a degenerate case of said function where ϕ remains constant. Intuitively it follows that to establish a spiral structure as the FFH's minimum-energy deformed configuration we must modulate its parameters to generate a monotonic continuous stiffness profile and thus a logarithmic deformation along its length. In plants and animals, this characteristic varying stiffness profile is accomplished by linearly tapering the limb's radius, which is a good match for systems that grow. While biologically practical, in robotic systems this method of varying stiffness makes it increasingly difficult to integrate actuators and sensors along the manipulator's length, and almost completely removes the ability to do so at the manipulator's most distal point.

Instead, we emulate the aforementioned stiffness profile by utilizing a novel variant of the FFH, whose cross-sectional width, and thus area moment of inertia, varies linearly along a shape-similar extrusion profile as shown in Fig. 4. The revolute joint approximation of FFH deformation

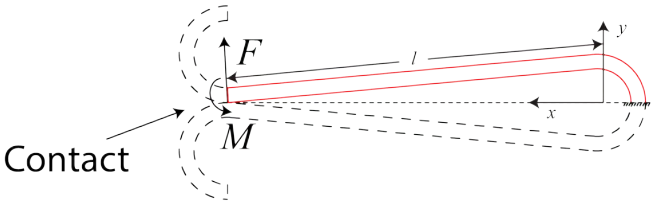

Fig. 3: Free body diagram of the approximation of an FFH segment as a cantilevered beam. Note that once the two segments are in contact there is a reaction force which will act on the following segment, thereby sequentially deforming the FFH [19]

models the deflection δ of an individual segment of the FFH as an isotropic cantilevered beam under the action of a free-end load until contact is made with an opposing segment as seen in Fig. 3. Thus, the hinges deflection can be simplified as a revolute joint with a rotation angle equivalent to the summation of deflection angles of the two opposing segments [19]. Due to the FFH's constant cross-section, and thus stiffness profile, all segments will deflect linearly with respect to the applied load and result in a circular profile.

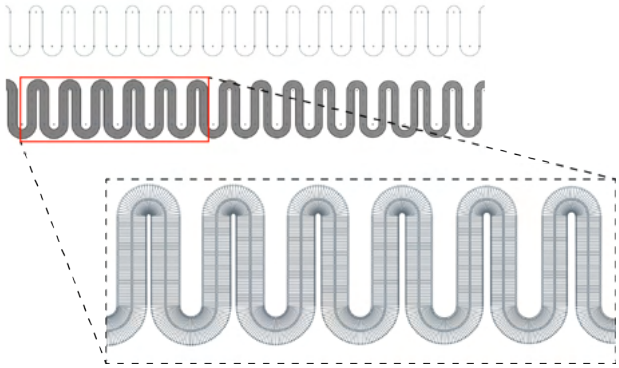

Fig. 4: Diagram showing the extrusion profile of the VAFFH and segment of the resultant geometry. To model the variable cross-section using CAD software we must treat the continuously varying cross-section as a series of profiles that maintain discrete transformations between one another. We then sequentially sweep these profiles to form a single body. The number of profiles defines the coarseness of the approximation to a continuous sweep, here a profile is added every 0.1 mm.

Eqs. (1-7) utilize Euler-Bernoulli beam theory to derive the deflection δ of a cantilever beam of span L with bending moment M and concentrated load P where the cross-section height $h(x)$, and thus area moment of inertia $I(x)$, varies linearly from h_0 at the fixed end to h_1 at the free end.

$$M = P(L-x) \tag{1}$$

This is an isostatic beam so the moment equation can be obtained as above.

$$\theta = \int_0^L \frac{P(L-x)}{E \cdot I(x)} \mathrm{d}x \tag{2}$$

We then divide the beam's stiffness and integrate across the length to obtain the beam's tangent. Eq. (3) describes how the area moment of inertia varies as a function of the position along the beam.

$$I(x) = \frac{b \cdot h(x)^3}{12} = \frac{b \cdot \left(h_0 + (h_1 - h_0)\frac{x}{L}\right)^3}{12} \tag{3}$$

Due to this variation we cannot remove $I(x)$ from the integral as with fixed cross section beams. Hence the tangent equation develops as shown below.

$$\theta = \frac{1}{E}\int_0^L \frac{12P(L-x)}{b \cdot \left(h_0 + \Delta h \frac{x}{L}\right)^3} \mathrm{d}x \tag{4}$$

$$\theta = \frac{6PL^3}{Eb\Delta h^2}\left(\frac{-\Delta hL + 2\Delta hx + h_0 L}{(\Delta hx + h_0 L)^2} + C_1\right) \tag{5}$$

Finally, we integrate the tangent to calculate the deflection.

$$\delta = \frac{6PL^3}{Eb\Delta h^2}\int_0^L \left(\frac{-\Delta hL + 2\Delta hx + h_0 L}{(\Delta hx + h_0 L)^2} + C_1\right) \mathrm{d}x \tag{6}$$

$$\delta = \frac{6P}{Eb\Delta h^2}\left(\frac{L(\Delta h + h_0)}{\Delta h(\Delta hx + h_0 L)} + \frac{2\ln(\Delta hx + h_0 L)}{\Delta h} + C_1 x + C_2\right) \tag{7}$$

We find that the linearly varying stiffness $E \cdot I(x)$ induces a deflection that varies as the natural log of the distance x from the fixed end. When applied in tandem with the revolute joint approximation we predict that the novel VAFHH will deform approximately logarithmically as a spiral. We demonstrate and validate these predictions using a 3D printed proof of concept model as shown in Fig. 5. We print the exoskeleton in PA12 nylon using Protolabs Inc. Multi Jet Fusion, which generates a part that is approximately isotropic. The exoskeleton is designed as a "U" shaped half-lumen and integrates two VAFFH in a parallel configuration to maintain out-of-plane stiffness. Tendon routing channels are placed running perpendicularly through the VAFFH segments. Additional tendon and camera routing channels are placed running through the exoskeleton's posterior surface as seen in Fig. 6.

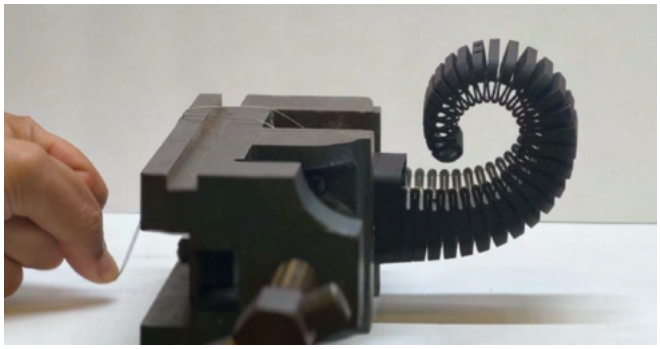

Fig. 5: Proof of concept demonstration of the flexure integrated exoskeleton. This clearly shows that by integrating the VAFFH the exoskeleton will maintain a deformation that varies logarithmically along its length, resulting in a spiral-like shape.

B. Elastomer Fabrication

We fabricate a molded silicone elastomer as the hyperelastic continuum body of our manipulator as shown in Fig.7. We utilize standard methods for GelSight-like elastomer fabrication as described by Adelson et al. [24], [22], [25] and utilize a PMMA mold to position and embed rigid camera mounts into the continuum as a bonded assembly. Silicone

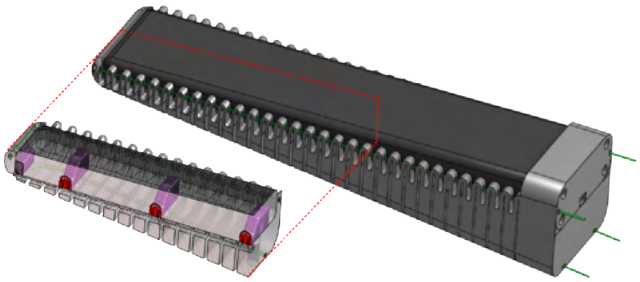

Fig. 6: Cross sectional view of the continuum manipulator. The actuation tendons and lens mounts are highlighted green and purple respectively.

in general has many advantageous material properties that indicate its use in soft robotic applications. For the tactile sensing applications, in which we are particularly interested, silicone is particularly useful because it is optically clear with a similar index of refraction to PMMA, a common lens material. Silicone can easily be cast into any shape using a mold and also provides excellent durability. Additionally, the specific material properties (abrasion resistance, elastic modulus, tear strength, etc.) of a given batch of elastomer, can be tuned by varying the ratio of the base and activator or adding a plasticizer like phenyl trimethicone. In spite of these advantageous properties, silicone's low surface energy poses an issue for designers. The low surface energy of silicone makes bonding to non-silicone materials exceedingly difficult, as silicone is prone to delamination. We utilize three methods to overcome this challenge when designing our manipulator.

- **Cleaning and Priming** the elastomer surface removes contaminants that would impede bonding and increases the surface energy of the elastomer to ensure better adhesion.
- **Preventative Design** should be used to mitigate areas of stress concentration where delamination is likely to originate. All hard edges and points should be chamfered or removed.
- **Mechanical Embedding** takes advantage of the liquid to solid phase transition that the elastomer undergoes during the casting and curing process to secure parts within the continuum. This process can be enhanced by adding a series of interweaving holes to increase the number of attachment points and better merge the two parts into a single component. Embedding is best used to create a rigid mounting point and enables efficient force transmission to the soft continuum.

IV. Experimental Results and Demonstrations

A. Force Characterization

We select a handle-grasping task to characterize the forcefulness of our continuum manipulator. Forcefulness is evaluated by measuring the transmitted force/torque through the three motions: screwing, hammering, and pulling as illustrated in Fig. 8.

The manipulator is mounted to a Franka Emika Panda robot arm to enable precise control during the experiment. A six-axis ATI force-torque sensor is then positioned within

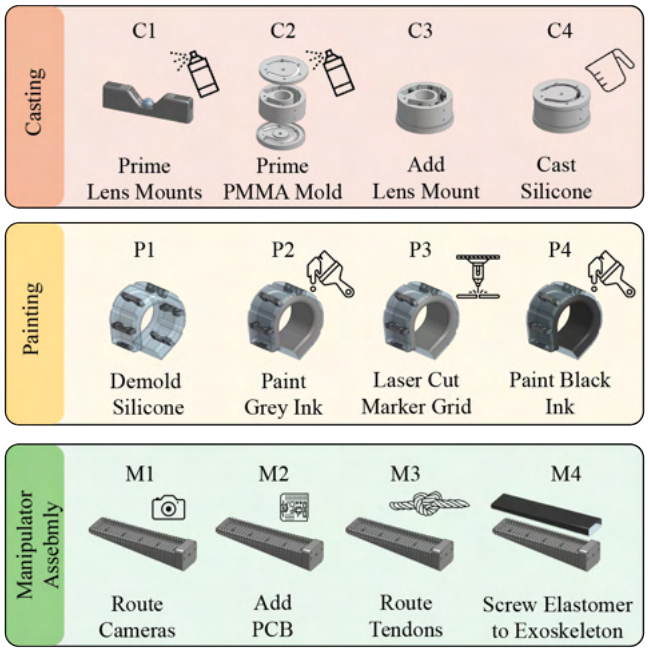

Fig. 7: Manufacturing process flow of the continuum manipulator, which includes elastomer mold design, casting embedded rigid components, and painting the reflective skin.

TABLE I: Force-Torque Characterization

Continuum Manipulator

Loading Scenario	Avg.	σ
Z-Axis Translation [N]	30.54	1.32
Z-Axis Rotation [Nm]	1.07	.19
X-Axis Rotation [Nm]	.82	.28

Weiss WSG32 w/GelSlim 3.0

Loading Scenario	Avg.	σ
Z-Axis Translation [N]	18.28	2.81
Z-Axis Rotation [Nm]	.53	.01
X-Axis Rotation [Nm]	.13	.04

the robot arm's workspace using a fixture with switchable magnets. To begin the experiment, the manipulator is guided to a handle attached to the force-torque sensor while the robot arm is in gravity-compensation mode. The servos in the manipulator are commanded to rotate a fixed distance using position control, thus initiating a grasp. The robot is then commanded to rotate or translate about a given axis, forces and torques are then measured until the grasp fails. A grasp is determined to have failed when the recorded value is no longer monotonically increasing. Data is recorded from the sensor using the ATI Net F/T interface. We utilize a selection of five randomly generated handle contours, shown in Fig. 9, to simulate the variance found in handles on objects in the human environment. Data is collected for each loading scenario and handle shape across five trials, the trial sets are then aggregated to generate an average force or torque value and standard deviation. Data is subsequently collected for a parallel jaw gripper for comparison. We use a Weiss WSG32 electronic gripper with two GelSlim 3.0 tactile fingers attached [24].

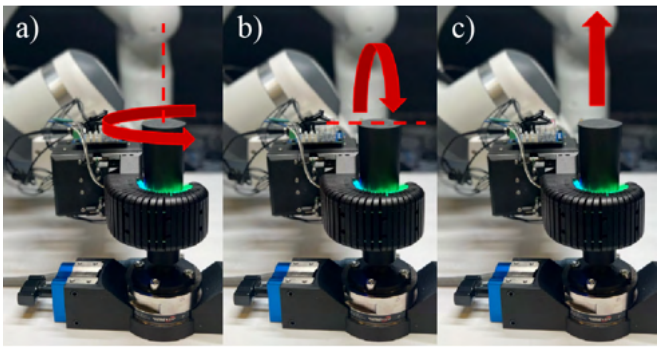

Fig. 8: a) *Screwing*: Rotations about the Z-axis, b) *Hammering*: Rotations about the X-axis, c) *Pulling*: Translations along the Z-axis

Fig. 9: Diagram of the selection of handle contours used for force-torque characterization. The contour line has been parametrized as a curve defined by a quadratic polynomial. The coefficients of the polynomial are randomized within a bounded range to generate a cross-section which is subsequently revolved around a central axis to generate the handle model.

Table I details the results of these tests. We find that the overall the continuum manipulator is approximately twice as forceful as the parallel jaw gripper. The manipulator successfully applies large translational forces along the Z-axis. The enhanced frictional contact enabled by the compliant, hyper-elastic anterior surface, induces a large resistance to the shear forces that develop along the internal faces of the manipulator. Since there are no additional rigid geometric interferences (as in the hammering case) to assist in maintaining the grasp, the grasp is purely held by the compliant body's deformation. This is in contrast with the hammering motion (rotations about the X-axis) which enables the application of torques even when the grasp does not fully envelope the handle. Because there is a geometric interference between the handle and the manipulator, as long as the actuators can maintain the manipulator's stiffness and the grasp does not fully open, torques can still be applied. The screwing motion falls in between these two in terms of the magnitude of forcefulness. Interestingly, the manipulator can only maintain torques for rotations that follow the direction of its spiral, in the opposite direction the manipulator will quickly detach from the handle. This is an inversion of the "universality" that scale-invariant approaches seemed to afford and demonstrates that the functional trade-off for taking advantage of scale-invariant behaviors is that they are in fact directional.

The amount of force supplied by the manipulator during these tasks is largely modulated by the surface condition of both the manipulator's contact region and the contacted object. It is expected that rougher contact patches would

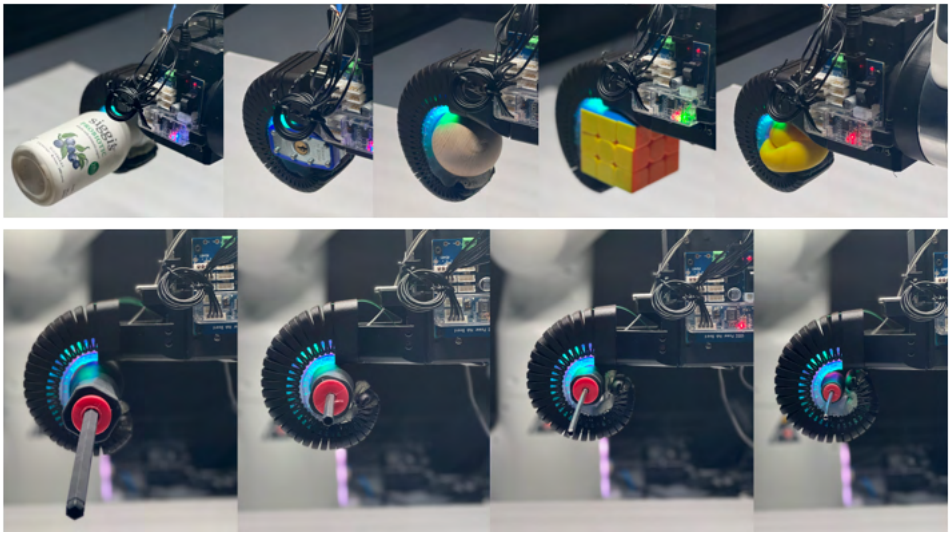

Fig. 10: **Grasp Compliance:** the continuum manipulator grasps various differently shaped everyday object. *From left-to-right:* a bottle, lock, wooden ball, Rubiks cube, and rubber duck. This ability to comply and conform to arbitrary geometries enables a diversity of enveloping grasps, from prismatic to spherical. **Scale Invariance:** several different sizes of hex screwdriver are enveloped in the spiral-like grasp of the manipulator.

adhere more readily to the hyper-elastic elastomer surface because of the increased contact area. While the manipulator provides sufficient force for handling household objects, to perform forceful tasks requiring even larger wrenches, for example: lifting objects heavier than a few kilograms, the manipulator would need to be further optimized for durability and force transmission. The elastomer surface could be replaced with a textile-based tactile sensor, for example, which would more readily resist gouging and delamination with regular wear. That being said, increased forcefullness would likely come at the cost of reduced compliance and sensing resolution since a material's durability is directly correlated with its elasticity [26].

B. Scale Invariance, Compliance, and Tactile Sensing

We further illustrate the scale-invariant and compliant properties of the continuum manipulator in Fig. 10 which illustrate several example grasps. While the manipulator demonstrates impressive abilities, it is not without its weaknesses. The length of the manipulator limits size of objects that can be grasped to objects with a radius less than three centimeters.The scale-invariant principles we utilize develop a directionality to the grasp performance that is undesirable. Additionally, because of the need to maintain the hyper-elastic properties of the anterior region, the cameras used for tactile sensing must be kept small. The small sensing region of the camera records data from a small field of view. This in turn makes it difficult to infer global information using the aggregated tactile feedback. While tactile feedback is traditionally a local method of feedback it has been shown useful for proprioception in addition to exteroception [22], [27]. The manipulators lack of a rigid reference frame results in reduced stability when utilizing model-based algorithms as well. When attempting to measure shape and detect incipient using the algorithms described by Dong et al.[25], the manipulator was only able to do so using a static pre-established grasp with small relative motion between the manipulator and the grasped object. For larger relative motions, these models, unsurprisingly, failed, since they assumed the former measurement conditions.

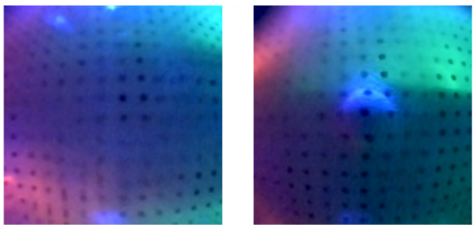

Fig. 11: Tactile Sensing: the raw tactile image of the manipulator is shown before and after a small bearing is pressed to its surface.

V. Conclusions

We present a novel high-resolution tactile enabled hybrid rigid-soft continuum manipulator design that is forceful, compliant, inherently safe, and easily controllable. Using Euler-Bernoulli beam theory and geometric inference we develop and describe the VAFFH, a novel variant of the FFH compliant mechanism. We integrate the VAFFH into the manipulator's design to develop a compliance profile that defines an approximately scale-invariant deformation along the length of the manipulator. We describe the design of the continuum manipulator and present methods to address the current challenges posed by traditional soft robotic materials. We evaluate the forcefulness of our manipulator using a selected grasping task and compare its performance to a traditional parallel jaw gripper. We demonstrate the adaptability of the manipulator by grasping irregularly shaped everyday objects and discuss the manipulator's limitations. In future work we anticipate developing tactile sensing-enabled manipulators in compliant and forceful form factors.

VI. Aknowledgment

This work is financially supported by the Toyota Research Institute. The authors would like to thank Edward Adelson for their feedback on the design and implementation of the proposed gripper.

References

[1] H. Wang, M. Totaro, and L. Beccai, "Toward perceptive soft robots: Progress and challenges," *Advanced Science*, vol. 5, p. 1800541, 07 2018.

[2] J. Shintake, V. Cacucciolo, D. Floreano, and H. Shea, "Soft robotic grippers," *Advanced Materials*, vol. 30, no. 29, p. 1707035, 2018. [Online]. Available: https://onlinelibrary.wiley.com/doi/abs/10.1002/adma.201707035

[3] W. Dou, G. Zhong, J. Cao, Z. Shi, B. Peng, and L. Jiang, "Soft robotic manipulators: Designs, actuation, stiffness tuning, and sensing," *Advanced Materials Technologies*, vol. 6, no. 9, p. 2100018, 2021. [Online]. Available: https://onlinelibrary.wiley.com/doi/abs/10.1002/admt.202100018

[4] X. Chen, X. Zhang, Y. Huang, L. Cao, and J. Liu, "A review of soft manipulator research, applications, and opportunities," *Journal of Field Robotics*, vol. 39, no. 3, pp. 281–311, 2022. [Online]. Available: https://onlinelibrary.wiley.com/doi/abs/10.1002/rob.22051

[5] Y. Zhang and W. Gruver, "Definition and force distribution of power grasps," in *Proceedings of 1995 IEEE International Conference on Robotics and Automation*, vol. 2, 1995, pp. 1373–1378 vol.2.

[6] E. Brown, N. Rodenberg, J. Amend, A. Mozeika, E. Steltz, M. R. Zakin, H. Lipson, and H. M. Jaeger, "Universal robotic gripper based on the jamming of granular material," *Proceedings of the National Academy of Sciences*, vol. 107, no. 44, pp. 18 809–18 814, 2010. [Online]. Available: https://www.pnas.org/doi/abs/10.1073/pnas.1003250107

[7] Animal Images, "African elephant trunk, lake manyara," 2018. [Online]. Available: https://pixels.com/featured/african-elephant-trunk-lake-manyara-animal-images.html

[8] Arjan Haverkamp, "Parsons' chameleon," 2011. [Online]. Available: https://www.flickr.com/photos/46956042@N00/6079006842

[9] Grégory Thiell, "Octopus tentacle," 2011. [Online]. Available: https://www.flickr.com/photos/mcdux/5482383469/in/faves-denisgobo/

[10] Chris Smith, "Day 11: Seahorse spiral," 2013. [Online]. Available: https://www.flickr.com/photos/cjsmithphotography/8741292778

[11] Mark Horton Photography, "Drosera binata fibonacci," 2013. [Online]. Available: https://www.flickr.com/photos/markqpr/8563908823

[12] J. Burgner-Kahrs, D. C. Rucker, and H. Choset, "Continuum robots for medical applications: A survey," *IEEE Transactions on Robotics*, vol. 31, no. 6, pp. 1261–1280, 2015.

[13] P. Singh and C. M. Krishna, "Continuum arm robotic manipulator: A review," *Universal Journal of Mechanical Engineering*, vol. 2, pp. 193–198, 2014.

[14] Q. Guan, J. Sun, Y. Liu, N. M. Wereley, and J. Leng, "Novel bending and helical extensile/contractile pneumatic artificial muscles inspired by elephant trunk," *Soft Robotics*, vol. 7, no. 5, pp. 597–614, 2020, pMID: 32130078. [Online]. Available: https://doi.org/10.1089/soro.2019.0079

[15] Z. Xie, A. G. Domel, N. An, C. Green, Z. Gong, T. Wang, E. M. Knubben, J. C. Weaver, K. Bertoldi, and L. Wen, "Octopus arm-inspired tapered soft actuators with suckers for improved grasping," *Soft Robotics*, vol. 7, no. 5, pp. 639–648, 2020, pMID: 32096693. [Online]. Available: https://doi.org/10.1089/soro.2019.0082

[16] D. B. Camarillo, C. F. Milne, C. R. Carlson, M. R. Zinn, and J. K. Salisbury, "Mechanics modeling of tendon-driven continuum manipulators," *IEEE Transactions on Robotics*, vol. 24, no. 6, pp. 1262–1273, 2008.

[17] M. D. Kutzer, S. M. Segreti, C. Y. Brown, M. Armand, R. H. Taylor, and S. C. Mears, "Design of a new cable-driven manipulator with a large open lumen: Preliminary applications in the minimally-invasive removal of osteolysis," in *2011 IEEE International Conference on Robotics and Automation*, 2011, pp. 2913–2920.

[18] Z. Du, W. Yang, and W. Dong, "Kinematics modeling and performance optimization of a kinematic-mechanics coupled continuum manipulator," *Mechatronics*, vol. 31, pp. 196–204, 2015. [Online]. Available: https://www.sciencedirect.com/science/article/pii/S0957415815001518

[19] L. Qiu, Y. Liu, Y. Yu, and Y. B. Bai, "Design and stiffness analysis of a pitch-varying folded flexure hinge (pffh)," *Mechanism and Machine Theory*, vol. 157, p. 104187, 2021. [Online]. Available: https://www.sciencedirect.com/science/article/pii/S0094114X20304043

[20] N. Lobontiu, J. Wight-Crask, and C. Kawagley, "Straight-axis folded flexure hinges: In-plane elastic response," *Precision Engineering*, vol. 57, pp. 54–63, 2019. [Online]. Available: https://www.sciencedirect.com/science/article/pii/S0141635919300637

[21] T. T. Hoang, P. T. Phan, M. T. Thai, N. H. Lovell, and T. N. Do, "Bio-inspired conformable and helical soft fabric gripper with variable stiffness and touch sensing," *Advanced Materials Technologies*, vol. 5, no. 12, p. 2000724, 2020. [Online]. Available: https://onlinelibrary.wiley.com/doi/abs/10.1002/admt.202000724

[22] Y. She, S. Q. Liu, P. Yu, and E. Adelson, "Exoskeleton-covered soft finger with vision-based proprioception and tactile sensing," in *2020 IEEE International Conference on Robotics and Automation (ICRA)*, 2020, pp. 10 075–10 081.

[23] A. Rodriguez and M. T. Mason, "Grasp invariance," *The International Journal of Robotics Research*, vol. 31, no. 2, pp. 236–248, 2012. [Online]. Available: https://doi.org/10.1177/0278364911430416

[24] I. H. Taylor, S. Dong, and A. Rodriguez, "Gelslim 3.0: High-resolution measurement of shape, force and slip in a compact tactile-sensing finger," in *2022 International Conference on Robotics and Automation (ICRA)*, 2022, pp. 10 781–10 787.

[25] S. Dong, W. Yuan, and E. H. Adelson, "Improved gelsight tactile sensor for measuring geometry and slip," in *2017 IEEE/RSJ International Conference on Intelligent Robots and Systems (IROS)*, 2017, pp. 137–144.

[26] S.-I. Moon, I.-J. Cho, C. Woo, and W.-D. Kim, "Study on determination of durability analysis process and fatigue damage parameter for rubber component," *Journal of Mechanical Science and Technology*, vol. 25, pp. 1159–1165, 05 2011.

[27] S. Q. Liu and E. H. Adelson, "Gelsight fin ray: Incorporating tactile sensing into a soft compliant robotic gripper," 2022. [Online]. Available: https://arxiv.org/abs/2204.07146